processes

MDPI

Article

Design and Implementation of Small Modular Amphibious Robot System

Fushen Ren and Zhongyang Wang *

Sanya Offshore Oil and Gas Research Institute, Northeast Petroleum University, Sanya 572025, China; renfushen@126.com

* Correspondence: wzy1719393666@126.com

Abstract: Various marine engineering facilities have been eroded by marine organisms and wind waves for a long time, resulting in different types of damage to the surface of marine engineering facilities, such as the pile legs of offshore platforms. Therefore, in order to carry out safety inspections and other work on marine engineering facilities, a small amphibious robot structure system and a set of control systems adapted to it are independently developed. Various problems such as the modular design of the structure, composite motion mode, adsorption stability, wall adaptability of the crawling mode, and flaw localization have been solved by means of three-dimensional modeling, mechanical analysis, simulation, and electronic design. At the same time, a set of control systems including hardware and software is developed for the amphibious robot. In order to improve the stability and efficiency of the amphibious robot working underwater, a sliding mode control algorithm based on the exponential reaching law and saturation function is designed. For the fixed depth and fixed heading control functions, the sliding mode control algorithm and the PID control algorithm are simulated and compared. Finally, several types of experiments are carried out for the amphibious robot. The simulation and experimental results show that all the functions of the amphibious robot meet work requirements, such as the motion performance of the composite motion mode. Compared with the PID control algorithm, the sliding mode control algorithm has a faster response speed and better stability, which is conducive to the efficient and stable work of the amphibious robot underwater.

Keywords: amphibious robot; ROV; magnetic adsorption crawler; control system; sliding mode control algorithm; simulation

Citation: Ren, F.; Wang, Z. Design and Implementation of Small Modular Amphibious Robot System. *Processes* **2024**, *12*, 2355. https://doi.org/10.3390/pr12112355

Academic Editor: Anthony Rossiter

Received: 21 September 2024
Revised: 18 October 2024
Accepted: 22 October 2024
Published: 27 October 2024

1. Introduction

The ocean is a natural treasure rich in resources. There are many kinds of resources such as natural gas, fish, and oil in the ocean [1]. With the progress of science and technology, resources on land have been unable to meet the needs of human beings. In order to explore and exploit marine resources, various engineering facilities have been developed and applied, such as offshore platforms, ships, underwater pipelines, etc., as shown in Figure 1. During the working process, engineering facilities are continuously eroded by seawater, sea breeze, and marine organisms, resulting in cracks and wear on the surface of the engineering facilities. Therefore, in order to prolong the service life of engineering facilities, the safety inspection of engineering facilities is carried out regularly. At present, the safety inspection of most engineering facilities is still completed by humans. With the development of intelligent equipment, ROVs are gradually replacing humans to complete related work.

Figure 1. Ocean platform.

Underwater robots are divided into three main categories [2]: Human-Occupied Vehicles (HOVs), Autonomous Underwater Vehicles (AUVs), and Remote-Operated Vehicles (ROVs). Among them, HOVs can carry workers into the deep sea to carry out salvage, scientific research, and other tasks. Hsowever, HOVs have the disadvantages of high cost, large volume, inflexible movement, and a large risk factor. At present, countries such as China, Japan, the United States, and Russia have the ability to independently develop deep-sea manned submersibles [3], for example, Limiting Factor and Alvin in the United States, Fendouzhe Striver and Jiaolong in China, and Rus and consul in Russia [4]. Compared with HOVs, AUVs have the ability of autonomous movement, but AUVs have some disadvantages such as unstable signal transmission and limited working time and load. With the rapid development of AUVs, some countries have developed a variety of AUVs [5], such as Orca and Manta in the United States, Explorer and Merman300 in China, Harpsichord−1R in Russia, and A9-S in France [6–8]. Compared with HOVs and AUVs, ROVs are more suitable for working in the shallow sea area and also have many advantages such as being flexible and small, easy to operate and control, expandable, and easy to maintain. Several robot manufacturing companies have developed various types of ROVs [9–11], including observation-type ROVs, operation-type ROVs, and bionic-type ROVs. Zhang et al. [12], Zhang et al. [13], and Yuan et al. [14] developed a shallow water observation-level small ROV with a lightweight and streamlined appearance, which is mainly used for underwater reconnaissance and environmental monitoring. Cui et al. [15], Cao et al. [16], and Wang et al. [17] designed a frame-type ROV. The frame-type ROV is equipped with a variety of sensors and working tools to complete the inspection of ships and pipelines. In addition to the three types of underwater robots mentioned above, there is another type of robot, a crawling robot. Wang et al. [18] designed a crawling robot for underwater structure inspection. This robot adopts the wheel-footed moving method and the adsorption method of negative-pressure suction cups, which has the ability to adapt to irregular wall surfaces. Zhao et al. [19] designed a crawler wall-climbing robot based on the magnet adsorption method. The magnets are uniformly installed on the crawler on both sides of the robot to achieve the adsorption, movement, and detection of the robot and the ship wall. Huang et al. [20] designed and developed a wall-climbing robot for bridge disease detection based on negative-pressure adsorption. The adsorption structure adopts the combination of a centrifugal impeller and negative-pressure suction cups, and the moving mode adopts the combination of two fixed wheels and one universal wheel. Han et al. [21] designed a crawler wall-climbing robot. The robot contacts the metal wall by electromagnetic adsorption. The electromagnets are evenly installed on both sides of the crawler. Wang et al. [22] designed a flexible four-legged wall-climbing robot. A number of electromagnetic suction cups are installed at the end of the four feet of the wall-climbing robot so that it can surround and adsorb onto the tube wall and walk along the tube wall.

Wang et al. [23] designed an underwater cleaning robot. This robot adopts the design scheme of rotary brush cleaning, thrust adsorption, and wheeled movement. In summary, the advantages and disadvantages of the above three types of underwater robots and the crawling robots are summarized in Table 1.

Table 1. Summary of the advantages and disadvantages of different types of robots.

Type	Advantages	Disadvantages	Examples of Research Results
HOVs	Mainly work in the deep sea, engage in complex work tasks and scientific exploration, real-time observation, and operation by on-site personnel	Inflexible movement, large volume, high cost, and high risk	e.g., Limiting Factor and Alvin in the United States, Fendouzhe Striver and Jiaolong in China, and Mir and consul in Russia [3,4]
AUVs	High degree of autonomy, high degree of crypticity, versatility, and mainly work in the deep sea	Large volume, limited working time, unstable signal transmission, high cost, and limited load capacity	e.g., Orca and REMUS series in the United States, Explorer and CR series in China, and Harpsichord−1R and MMT series in Russia [5–8]
ROVs	Various types, flexible control, high safety, long operation time, and mature technology	No crawling motion mode, high operational technical requirements, limited working range, and mainly work in the shallow sea	e.g., Multi-series ROVs from different robot manufacturing companies [9–11], streamlined observation-level ROV [12–14], and frame detection ROV [15–17]
Crawling robots	Various types, able to complete difficult tasks, convenient operation, and strong adaptability	Limited load capacity, difficult to manufacture, and no floating motion mode	e.g., Wheel-footed crawling robot based on negative-pressure suction cups [18], permanent magnet adsorption crawler robot [19], electromagnetic adsorption crawler robot [20], flexible four-legged wall-climbing robot based on electromagnetic suction cups [22], and roller wall-climbing robot based on thrust adsorption [23]

The environment at the low depths of the ocean is very complex, and the ROV itself is also a nonlinear system. Therefore, the control difficulty of the ROV will be greatly increased. A good motion control algorithm is a prerequisite to ensure that the underwater vehicle can complete the task, which requires the robot to have the ability to quickly approach the target position and maintain stability after reaching the target position. In order to improve the stability of the ROV's underwater attitude, it is necessary to design a robust motion control algorithm. At present, the PID control algorithm has a simple structure and is applied in many fields [24–26], but the control effect is not ideal in the nonlinear system. The neural network control algorithm [27–29] has a complex structure, high hardware requirements, and unstable convergence results. For external interference and system uncertainty, the sliding mode control algorithm [30–32] has strong robustness. However, there is a chattering problem in this algorithm, which is an important problem to be solved. The methods to eliminate the chattering problem are summarized in Table 2.

In summary, it is difficult for the above research results to accomplish the work that exists both above and below water. A compound robot that can swim underwater and crawl on the metal wall is needed to complete the work in the above two environments. Therefore, a small modular amphibious robot was developed independently, and a matching control system was developed. The amphibious robot can complete the safety inspection and other work in the underwater part and the overwater part of the engineering facility. Various problems such as the modular design of the structure, composite motion mode, adsorption stability, wall adaptability of the crawling mode, stability and efficiency of the control system, automatic motion function of the floating mode, and flaw localization have been solved by means of three-dimensional modeling, mechanical analysis, simulation, and electronic design.

Table 2. Comparison of chattering elimination methods for sliding mode control.

Method	Advantages	Disadvantages
Introduce saturation function	The principle of turning symbolic function into linear function is simple and easy to implement	Large control errors may be introduced
Add a sliding mode observer	Estimate the system state and external interference to reduce the influence of the control variable on the system	The system needs better modeling and parameter adjustment, and the design and implementation are more complex
Combine with adaptive control	The controller parameters can be adjusted according to the dynamic changes in the system to adapt to uncertain external disturbance	The system requires ideal modeling and parameter adjustment, and the computational complexity is high
Introduce reaching law	The response speed is fast, and the approaching time is short	It is more complex to choose the expression form according to the system characteristics

Based on the modular design idea, the amphibious robot is composed of a floating robot system and a crawler chassis system. The various pieces of basic equipment are independent of each other and can be disassembled and replaced at any time. The floating robot system has reserved mounting holes for working equipment and can be equipped with different operating equipment according to operation requirement, such as cleaning guns, detection probes, and manipulators. The application of the modular design idea improves the reliability, flexibility, and scalability of the system and reduces the installation and replacement time of the equipment. The amphibious robot has two motion modes: underwater swimming and wall crawling. According to different working environment and task requirements, the motion mode can be switched freely, which improves the versatility of the system and the adaptability of application scenarios. By establishing the mathematical model of the two motion modes of the amphibious robot, the amphibious robot can swim with multiple degrees of freedom underwater through six thrusters and can also crawl with multiple degrees of freedom on metal walls through magnetic adsorption crawlers. The floating robot system adopted the design scheme of a small, lightweight, and streamlined appearance, which reduces the overall weight and volume, reduces the water flow and air resistance, and is also convenient to carry. In order to improve the stability of the crawling movement and reduce the risk of leaving the working wall, the crawler chassis system adopted the motor-driven method of a synchronous wheel and synchronous belt combination and the magnetic adsorption method of a connecting permanent magnet and synchronous belt. The minimum adsorption force and the type of permanent magnet were analyzed and determined by establishing a static model in crawling mode. In order to adapt to metal walls with different curvature, an adaptive structure based on a spring shock absorber and hinge was designed in the crawler chassis system. In order to prevent the slack of the synchronous belt, a tightening structure based on adjusting bolts and synchronous wheels was designed in the crawler chassis system.

In order to realize the motion function and other control functions of the amphibious robot, a complete set of control systems was designed independently, including a hardware system and software system, such as a small multi-function control main board, a remote control handle, a carrier communication module, overwater control software, an underwater control program based on RTOS, remote update program software, etc. This control system can realize all the functional requirements of the amphibious robot and realize the integrated design of high efficiency, real-time property, interactivity, and reliability of the control system. In order to improve the anti-interference ability and working stability of the amphibious robot in the complex underwater environment, a sliding mode control algorithm based on the combination of the exponential reaching law and saturation function was designed. The exponential reaching law and saturation function can accelerate the response speed of the system and improve the stability of the system. For the fixed depth and fixed heading control function, the control algorithm and PID control algorithm were simulated and compared. Finally, experiments were carried out on the

basic motion forms of the amphibious robot's two motion modes, the functional testing of the structure system and the control system, the control effect of the control algorithm, and the working simulation of the application scenario. The rationality of the structure design and the diversity of functions of the amphibious robot were verified by both simulation and experiments, and the flexibility and stability of the control system of the amphibious robot were tested in different motion modes.

2. System Composition and Principle

The amphibious robot system includes two parts: the structural system and control system, as shown in Figure 2. The technical parameters of the amphibious robot are shown in Table 3.

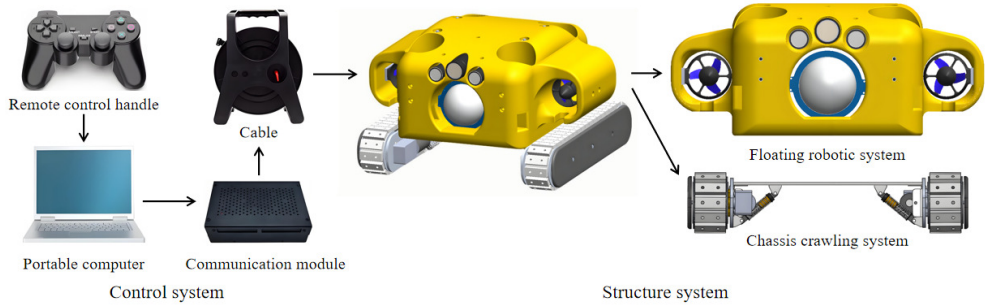

Figure 2. The amphibious robot system.

Table 3. Technical parameters of amphibious robot system.

Parameter Name	Parameter Value
The size of the floating robot system	375 mm × 500 mm × 210 mm
The weight of the floating robot system	12.5 KG
The size of the crawler chassis	425 mm × 452 mm ×100 mm
The weight of the crawler chassis	7.5 KG
Maximum working depth	100 m
Underwater maximum swimming speed	1.5 m/s
Maximum wall-climbing speed	3.5 m/min

The robot structure system adopts modular design [33], which is composed of a floating robot system and a crawler chassis system. The robot structure system has a swimming mode and crawling mode. The motion mode is switched for different working environments. The crawler chassis system contacts and crawls along the metal wall by magnetic adsorption. At the same time, the crawler chassis system has the ability to adapt to the wall surface for different curvatures of the metal wall. After removing the crawler chassis system, the floating robot system can swim and work independently underwater. The different devices in each system work independently of each other and can be removed and replaced at any time. The floating robot system reserves a hole position and can be equipped with different operating equipment according to operation requirement, such as cleaning guns, detection probes, and manipulators.

In the robot control system, the portable computer and the overwater control software can receive and display the status information of various devices and video pictures in real time and can also send some control commands to the underwater control system. The basic motion mode of the robot structural system and some sensors are controlled by the control handle. All electrical equipment is provided with power by the power supply system. The overwater control equipment and the robot structure system are connected by the cable system to realize the transmission of power and signals between them. The underwater control system is a comprehensive system that analyzes and processes various

instructions and realizes different control functions according to different instructions. In the following, each system is designed and analyzed in detail.

3. Structure System Design

3.1. Structure Design of the Floating Robot System

The role of the buoyancy module is to configure the amphibious robot system to a state of zero buoyancy or a very small positive buoyancy, ensuring that the control of different orientations and attitudes can be accomplished by using a small amount of thrust. In order to reduce the movement resistance of the system and improve the aesthetics of the system, the buoyancy module adopts a closed and streamlined design scheme, as shown in Figure 3. The buoyancy module is made of PVC foaming material with a density of 0.35 g/cm^3, and the material properties can meet the strength requirements at a depth of 300 m. In order to ensure that the amphibious robot can move and work stably underwater, the center of buoyancy is located directly above the center of gravity by optimizing the design of the buoyancy module and the installation position of other equipment. In order to carry different types of working devices in the future, the buoyancy module is designed as a structure whose buoyancy is greater than the total gravity of the amphibious robot by 2 KG. Through the design and calculation of the three-dimensional modeling software, the center of gravity coordinate of the amphibious robot is (1.1 mm, 2.4 mm, 17.7 mm), and the center of buoyancy coordinate is (0.4 mm, 1.9 mm, 92.4 mm), which ensures that the center of buoyancy is directly above the center of gravity. The parameters of the buoyancy module and other equipment of the amphibious robot are summarized in Table 4.

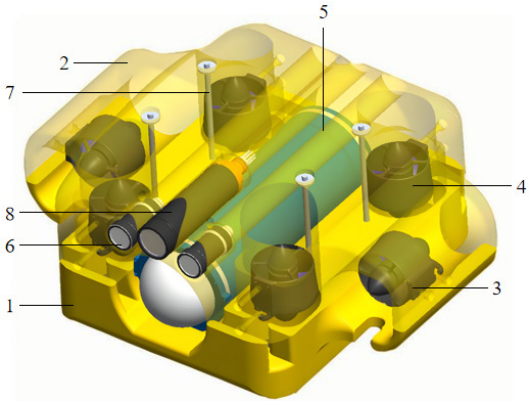

Figure 3. Three-dimensional model of the floating robot system. 1—the bottom half of the buoyancy module; 2—the top half of the buoyancy module (transparent state); 3—horizontal thruster; 4—vertical thruster; 5—control cabin; 6—underwater floodlight; 7—screw rod; 8—underwater camera.

Table 4. Gravity and buoyancy parameters of different subsystems.

Name	Gravity	Buoyancy
The amphibious robot system	200 N	220 N
The buoyancy module of the floating robot system	51 N	146 N
Other equipment of the floating robot system	74 N	53 N
The crawler chassis system	75 N	21 N

The front end of the buoyancy module is provided with three installation holes. Two underwater floodlights are installed in the holes on both sides to provide lighting for the front area of the structure system. The intermediate hole is the reserved installation hole, which is equipped with different working equipment according to the working task. At present, an underwater camera is installed in the middle hole to assist the pan–tilt camera. The floating robot system is designed and installed with six thrusters, including four vertical thrusters and two horizontal thrusters. The robot structure system can

complete the snorkeling movement, the forward and backward movement, the horizontal turning movement, the pitching movement, and so on, in the water.

The control cabin is the central system of the amphibious robot. The control cabin adopts a cylindrical design scheme, which has high-pressure resistance and a low processing cost. The 3D model of the control cabin is shown in Figure 4. The transparent protective window is made of acrylic material, and other components are made of aluminum alloy. The control cabin is equipped with three layers of circuit boards, multiple sensors, and a single-degree-of-freedom pan–tilt camera. The single-degree-of-freedom pan–tilt can adjust the pitch angle.

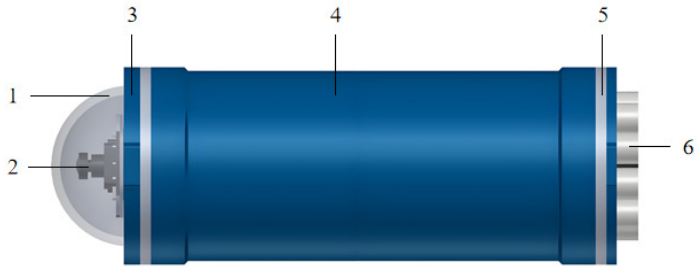

Figure 4. Three-dimensional model of the control cabin. 1—transparent protective window; 2—pan–tilt camera; 3—connecting circular plate; 4—cylindrical cabin; 5—connecting flange; 6—sealing hollow bolt.

The control cabin is the protection device of the underwater control system. For the sake of safety, the control cabin is simulated and analyzed [34]. In order to simulate the pressure environment of 100 m underwater, a pressure of 1.5 Mpa is applied to the outer surface of the control cabin. The simulation results of the control cabin are shown in Figure 5. The simulation results show that the maximum stress of the control cabin is distributed across the outer surface of the cylindrical cabin, and the value is 22.58 Mpa. The maximum deformation is distributed near the center of the transparent protective window, and the value is 0.097 mm. The safety factor of all components is calculated to be greater than 1.5. Therefore, the control cabin meets the strength requirement of 100 m underwater. Similarly, the simulation and analysis of other equipment of the robot structural system are carried out, and the results all meet the strength requirement of 100 m underwater.

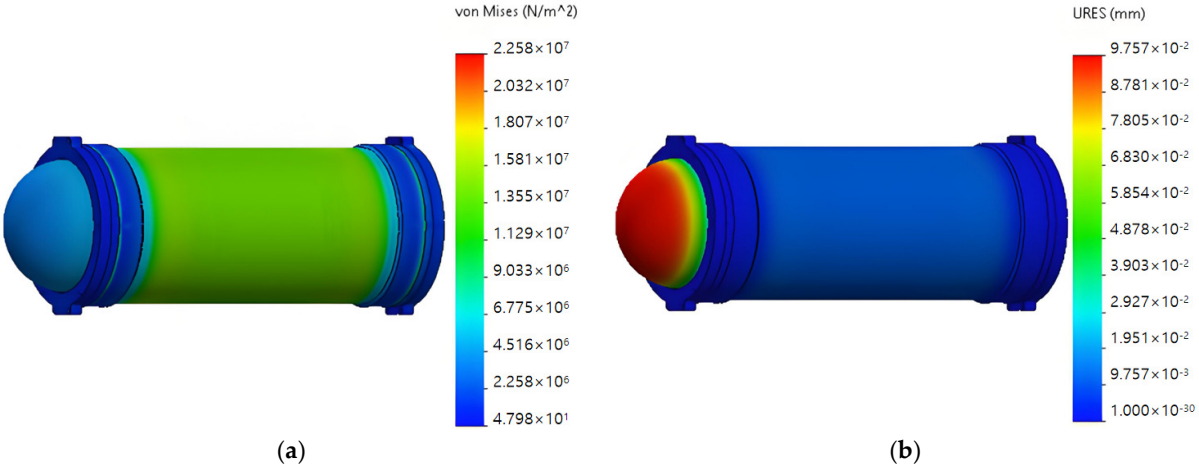

Figure 5. Simulation result diagram of the control cabin. (**a**) Stress result diagram; (**b**) deformation result diagram.

3.2. Structure Design of the Crawler Chassis System

In order to enable the amphibious robot to crawl and work on metal structures in different environments, with different curvatures, and with different tilt angles, a crawler

chassis system is developed independently. In order to improve the safety and stability of the amphibious robot in the crawling process, the magnetic adsorption scheme is selected for the adsorption mode, the crawler movement scheme is selected for the moving mode, and the motor drive scheme is selected for the driving mode.

The three-dimensional model and structure layout of the crawler chassis system are shown in Figure 6. The synchronous belt is made of polyurethane material, which has good wear and tensile properties. The synchronous wheel is made of aluminum alloy and designed to reduce weight. The magnetic adsorption module is mounted on the outer surface of the synchronization belt. The magnetic adsorption module is composed of a permanent magnet and yoke iron [35]. The function of the yoke iron is to reflect the magnetism of the back of the magnet and increase the magnetic force of the front of the magnet. The worm gear motor is selected as the waterproof motor that drives the crawler movement, with a maximum speed of 10 RPM and a maximum torque of 11 NM.

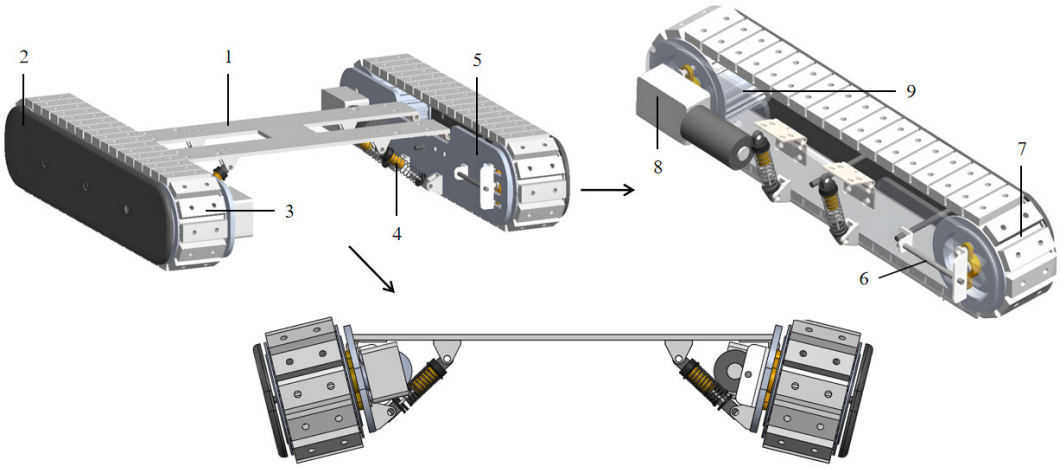

Figure 6. Three-dimensional model of the crawler chassis. 1—horizontal connection plate; 2—protective plate; 3—magnetic adsorption module; 4—spring shock absorber; 5—vertical connection plate; 6—tightening mechanism; 7—synchronous belt; 8—waterproof motor; 9—synchronous wheel.

To prevent the synchronous belt from becoming slack, a set of tightening structures is designed. The tightening structure includes fixed angle steel, sliding angle steel, a bolt, and a nut. Adjusting the bolt and nut makes the sliding angle steel and synchronous wheel move outward at the same time, which realizes the tightening function of the synchronous belt. For metal walls with different curvatures, the wall adaptive structure is designed, including hinges and spring shock absorbers. The horizontal connection plate and the vertical connection plate are flexibly connected by the hinge, and the spring shock absorber is connected with the horizontal connection plate and the vertical connection plate. In the initial state, the vertical connection plate and the horizontal connection plate are vertical. Under the action of the spring shock absorber, the crawler modules on both sides can be bent inward at different angles to adapt to metal walls with different curvatures, as shown in Figure 6. The crawler chassis system is connected to and disassembled from the floating robot system through the horizontal connection plate.

4. Control System Design

The robot control system is mainly composed of the overwater control system and the underwater control system, and the control system block diagram is shown in Figure 7.

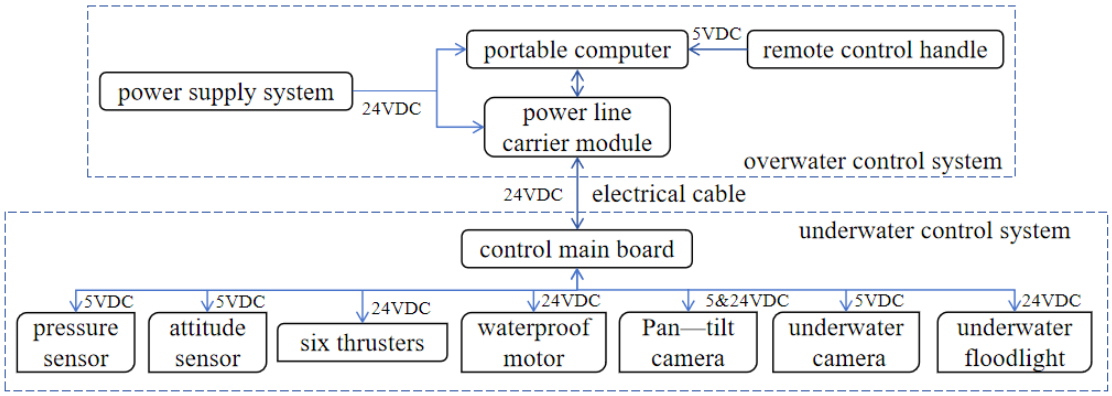

Figure 7. Control system block diagram.

4.1. Hardware Design of the Control System

In the overwater control system, the remote control handle is wired to a portable computer, and different control functions are assigned to the keys of the remote control handle by programming. The portable computer is connected to the structural system through the carrier module and the cable system. The control instructions of the remote control handle are transmitted to the underwater control system from the cable system. Different control instructions are analyzed by the underwater control system, and different control functions are realized.

The control main board is the core hardware of the underwater control system, as shown in Figure 8. The control main board is composed of three layers of circuit boards. The first-layer circuit board mainly includes the main control chip, a communication module, a power supply interface, and two underwater lighting interfaces. The second circuit board mainly includes two waterproof motor interfaces, a depth sensor module, and an attitude sensor module. The third-layer circuit board mainly consists of six thruster interfaces and electronic speed modules.

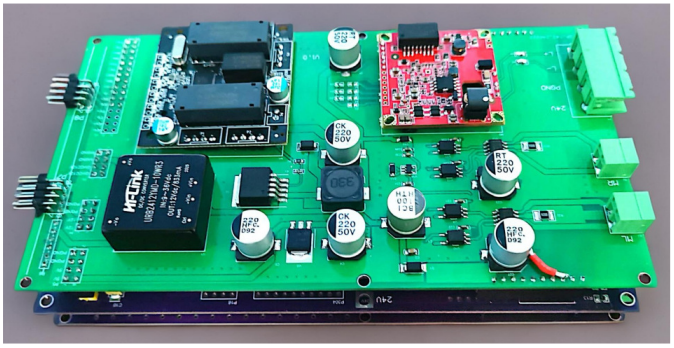

Figure 8. Control main board.

The main control chip STM32F103VET6 is selected as the controller, which has a high-performance core and is equipped with a variety of interfaces. This chip can meet the needs of the robot control system. The data collected by the attitude sensor and the depth sensor are transmitted to the MCU through the IIC interface. Six thrusters, two underwater floodlights, two waterproof motors, and one pan–tilt motor are controlled by the MCU through 11 PWM channels. The pan–tilt camera is connected to the MCU through the RS485 interface.

4.2. Software Design of the Control System

The software design of the control system mainly includes the following parts: an underwater control program based on RTOS, overwater control software, and remote update program software.

The underwater control program is developed by STM32CubeMX and Keil. The tasks of the underwater control system consist of four main aspects: (1) the task of communication and information transmission between the control main board and the portable computer, (2) the task of the automatic control of the amphibious robot, (3) the task of sensor data acquisition and processing, and (4) the task of the basic motion control and sensor control of the amphibious robot. In order to ensure the coordinated operation of different tasks, FreeRTOS is introduced into the underwater control system. FreeRTOS allocates different threads for different tasks and assigns priority to different tasks. The FreeRTOS program design flow chart is shown in Figure 9.

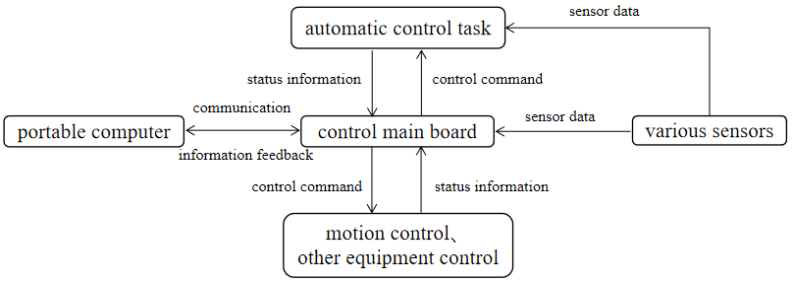

Figure 9. FreeRTOS flow chart.

In order to quickly update the program in the control main board without destroying the sealing of the control cabin, a remote update program software was developed, as shown in Figure 10. The program in the control main board is remotely upgraded by the portable computer through the cable system. After the power system is turned on, the remote upgrade program software is run, and the connection with the control main board is established through the local area network. Then, after the control main board receives the upgrade command, the flash area of the application part is erased; the new program file is downloaded to the corresponding address. The above process implements a remote update program.

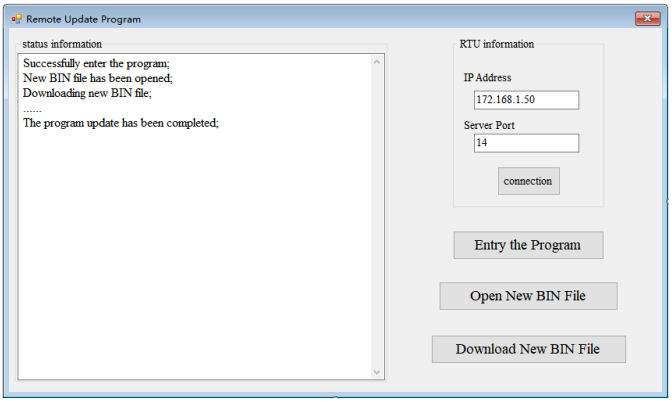

Figure 10. Remote upgrade program software.

In order to realize the remote control and data transmission between the overwater control system and the underwater control system, an overwater control software is designed. The display content of the software includes the position and posture information of the amphibious robot, the state information of different devices, and the instruction input module. All the input instructions are synthesized into a string according to a specific format, and then, the string is sent to the control main board. The string is parsed by the control main board, and a different control program is executed. Finally, the data and other information collected by the sensor are transmitted to the overwater control software in a specific format through the control main board and displayed.

5. Static Analysis of Amphibious Robot in Crawling Mode

The amphibious robot has two working environments in crawling mode: in the water and in the air. Since the underwater gravity of the amphibious robot is almost zero, the probability of instability is higher when the amphibious robot crawls on the wall in the air. When the amphibious robot is stationary on the wall, there are two main types of instability conditions that are most likely to occur: slip and overturning. Therefore, the static model of the amphibious robot in the critical state of the above two instability conditions is analyzed [36].

5.1. Critical State for Downward Slip

As shown in Figure 11, when the amphibious robot is stationary on the wall, the forces it receives include gravity G, friction F_f, the supporting force F_N of the wall on the amphibious robot, and total magnetic adsorption force F_M. When the component force of gravity (parallel to the wall) is greater than the friction force, the amphibious robot will slide down the wall.

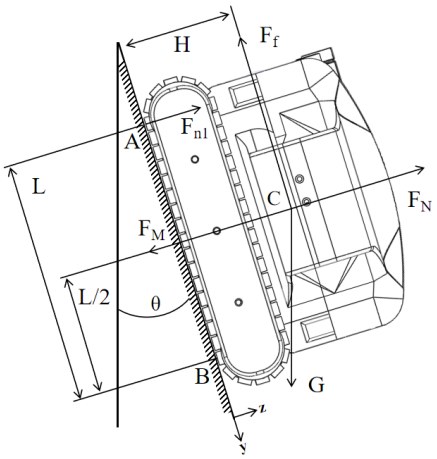

Figure 11. Force analysis diagram.

Therefore, in order to prevent the amphibious robot from sliding down the wall, the following conditions must be met:

$$F_f \geq G\cos\theta \tag{1}$$

$$F_f = \mu F_N \tag{2}$$

where θ is the wall inclination angle and μ is the friction coefficient.

The amphibious robot is balanced in the Z direction, and the following equation can be obtained:

$$F_M + G\sin\theta = F_N \tag{3}$$

Assuming that the adsorption force of each permanent magnet is the same, then

$$F_M = 2nF_m \tag{4}$$

where F_m is the adsorption force of a single permanent magnet and n is the number of permanent magnets a single side crawler contacts with the wall.

Combining the above four formulas, the following inequality is obtained:

$$F_m \geq \frac{G\cos\theta}{2\mu n} - \frac{G\sin\theta}{2n} \tag{5}$$

In the critical state of downward sliding, when the adsorption force of a single permanent magnet satisfies Inequality (5), the robot will not slide along the wall.

5.2. Critical State for Longitudinal Overturning

As shown in Figure 11, the contact points between the front end and the back end of the crawler and the wall are points A and B, respectively. Under the action of gravity, the amphibious robot has a tendency to overturn at around point B. The synchronous belt is a flexible mechanism, which cannot transmit a bending moment. Therefore, when the support force of the wall to the magnet at the front end of the crawler is greater than zero, the amphibious robot will not overturn.

Assuming that the amphibious robot is in equilibrium at point B, the torque balance equation is as follows:

$$(2F_mL + G\sin\theta * L/2) - (2F_{n1}L + G\cos\theta * H) = 0 \tag{6}$$

where the distance between point A and point B is L, the support force of the working wall to the first magnet is F_{n1}, and the vertical distance from the center of gravity of the amphibious robot to the wall is H.

In order to ensure that the amphibious robot does not overturn longitudinally, the following condition needs to be met:

$$F_{n1} \geq 0 \tag{7}$$

Combining Equations (6) and (7), the following inequalities are obtained:

$$F_m \geq \frac{GH\cos\theta}{2L} - \frac{G\sin\theta}{4} \tag{8}$$

In the critical state of longitudinal overturning, in order to ensure that the amphibious robot will not flip and leave the working wall, the adsorption force of a single permanent magnet needs to satisfy Inequality (8).

5.3. Numerical Calculation and Analysis

Based on the static analysis above, it can be seen that in order to ensure that the amphibious robot does not lose its stability, the adsorption force of a single permanent magnet needs to satisfy Inequalities (5) and (8).

In the two inequalities, G = 200 N, H = 150 mm, L = 330 mm, μ = 0.4, and n = 12. The two formulas are numerically calculated, and the calculation results are shown in Figure 12.

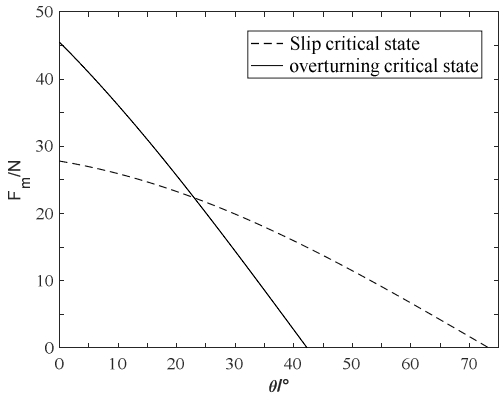

Figure 12. The relation curve between F_m and θ.

According to Figure 12, when the wall inclination angle is 0 degrees, the adsorption force of a single magnet reaches the maximum value under two critical instability states, which are 28 N and 46 N. Due to the instability of the working environment, a safety factor of 1.3 was taken. Therefore, in order to ensure that the amphibious robot does not slip and overturn on the working wall, the adsorption force of a single magnet needs to be greater than 60 N.

5.4. Design and Experiment of the Permanent Magnet

Comparing and analyzing the materials of permanent magnets [37], the NdFeB material is the most magnetic permanent magnet at present and has high cost performance and convenient processing and manufacturing. Therefore, the NdFeB material is selected as the permanent magnet [38]. Due to the limitation of the installation size of the permanent magnet on the synchronous belt, the external size of the permanent magnet is designed to be 50 mm × 18mm × 5 mm, and there are two countersunk holes with a spacing of 25 mm. The simulation of and experiments on the permanent magnet with the above size are carried out. The results show that the adsorption force generated by the permanent magnet is about 70 N, which meets the crawling needs of the amphibious robot. The experimental results are shown in Figure 13.

Figure 13. Simulation of and experiment on adsorption force.

6. Establishment of Mathematical Model of Amphibious Robot in Floating Mode

In order to accurately and stably control the amphibious robot swimming underwater, it is very important to establish a mathematical model of the amphibious robot. The mathematical model of the amphibious robot mainly includes the kinematics model and dynamics model.

6.1. Kinematics Model

In order to establish the mathematical model of the amphibious robot and study its underwater motion, the coordinate system needs to be defined and selected first. In this paper, the earth coordinate system (O_E-ξηζ) and the motion coordinate system (O_G-XYZ) are established, as shown in Figure 14. The motion parameters of the amphibious robot defined in the two coordinate systems are shown in Table 5.

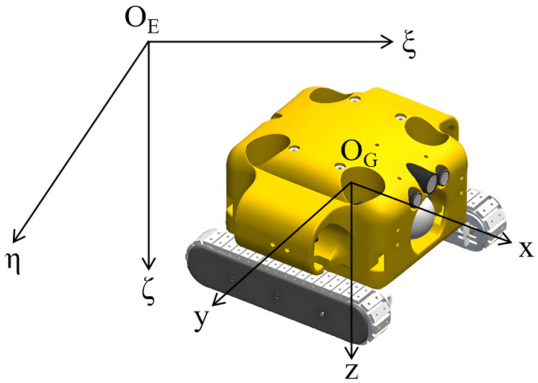

Figure 14. Diagram of coordinate system.

Table 5. Motion parameters of amphibious robot.

Linear Motion	Linear Velocity	Location	Force	Rotational Motion	Angular Velocity	Attitude	Torque
x-axis	u	x	X	x-axis	p	φ	K
y-axis	v	y	Y	y-axis	q	θ	M
z-axis	w	z	Z	z-axis	r	ψ	N

In order to easily express the motion characteristics of the amphibious robot, the earth coordinate system and the motion coordinate system are converted. The transformation relationship is as follows:

$$\dot{\eta} = Rv \tag{9}$$

where $\eta = [x,y,z,\varphi,\theta,\psi]^T$; $v = [u,v,w,p,q,r]^T$.

R is the transformation matrix between two coordinate systems, which is defined as follows:

$$R = \begin{pmatrix} R_1 & 0_{3*3} \\ 0_{3*3} & R_2 \end{pmatrix} \tag{10}$$

R_1 and R_2 are obtained by three rotations and transformations of Euler angles ϕ, θ, and ψ. Therefore, the complete kinematics model of the amphibious robot [39] is as follows:

$$\begin{bmatrix} \cos\theta\cos\psi & -\cos\varphi\sin\psi+\sin\varphi\sin\theta\cos\psi & \sin\varphi\sin\psi+\cos\varphi\sin\theta\cos\psi & 0 & 0 & 0 \\ \cos\theta\sin\psi & \cos\varphi\cos\psi+\sin\varphi\sin\theta\sin\psi & -\sin\varphi\cos\psi+\cos\varphi\sin\theta\sin\psi & 0 & 0 & 0 \\ -\sin\theta & \sin\varphi\cos\theta & \cos\varphi\cos\theta & 0 & 0 & 0 \\ 0 & 0 & 0 & 1 & \sin\varphi\tan\theta & \cos\varphi\tan\theta \\ 0 & 0 & 0 & 0 & \cos\varphi & -\sin\varphi \\ 0 & 0 & 0 & 0 & \sin\varphi\sec\theta & \cos\varphi\sec\theta \end{bmatrix} \begin{bmatrix} u \\ v \\ w \\ p \\ q \\ r \end{bmatrix} = \begin{bmatrix} \dot{x} \\ \dot{y} \\ \dot{z} \\ \dot{\varphi} \\ \dot{\theta} \\ \dot{\psi} \end{bmatrix} \tag{11}$$

6.2. Dynamic Model

The amphibious robot is a strongly coupled nonlinear system. In order to model and calculate more conveniently, the amphibious robot system is simplified: (1) assume that the center of gravity of the amphibious robot coincides with the origin of the motion coordinate system; (2) assume that the gravity and buoyancy of the amphibious robot are equal and the center of buoyancy coincides with the center of gravity; and (3) assume that the amphibious robot is a rigid body with a completely symmetrical structure and stable underwater motion speed. According to Newton's law and momentum theorem, the dynamic model of the amphibious robot [40] is as follows:

$$M\dot{v} + Cv + Dv + g + f = \tau \tag{12}$$

where M is the inertia matrix; C is the Coriolis force and centripetal force matrix; D is the fluid damping matrix; g is the static force; f is the external interference force; and τ is the driving force.

When the amphibious robot moves underwater, the coupling phenomenon will occur between different degrees of freedom, which makes the solution of the mathematical model very complicated. Therefore, in order to stabilize the underwater motion of the amphibious robot and facilitate the design of controller, the mathematical model is decoupled in degrees of freedom [41]. The decoupling method uses single-degree-of-freedom decoupling to decompose the motion of the underwater robot into six single-degree-of-freedom motions.

When the amphibious robot completes the forward and backward motion (linear motion along the X-axis direction) underwater, the velocity and acceleration of other degrees of freedom are both 0, and the dynamic equation of the amphibious robot is simplified to the following equation [42]:

$$(m - X_{\dot{u}})\dot{u} + \left(X_u + X_{u|u|}\left|u\right|\right)u + f = X \tag{13}$$

Similarly, the dynamic equations of the other five degrees of freedom are simplified as follows:

$$\begin{cases} (m - Y_{\dot{v}})\dot{v} + \left(Y_v + Y_{v|v|}\left|v\right|\right)v + f = Y \\ (m - Z_{\dot{w}})\dot{w} + \left(Z_w + Z_{w|w|}\left|w\right|\right)w + f = Z \\ \left(I_x - K_{\dot{p}}\right)\dot{p} + \left(K_p + K_{p|p|}\left|p\right|\right)p + f = K \\ \left(I_y - M_{\dot{q}}\right)\dot{q} + \left(M_q + M_{q|q|}\left|q\right|\right)q + f = M \\ (I_z - N_{\dot{r}})\dot{r} + \left(N_r + N_{r|r|}\left|r\right|\right)r + f = N \end{cases} \tag{14}$$

7. Design and Simulation of Sliding Mode Control Algorithm

7.1. Design of Sliding Mode Controller

The essence of sliding mode control is a model-based nonlinear control method that ensures stability through sliding mode theory. The principle of sliding mode control [43] is to design a sliding mode that is independent of the parameters and disturbances of the system. The control quantity is continuously switched through a certain function rule, so that the system is constrained on the switching surface, and then automatically slides to the sliding mode surface. Therefore, sliding mode control has good robustness. The existence of sliding mode is a necessary and sufficient condition for the stability of the system. The stability of the system is usually proved by Lyapunov stability theory [44].

The design of the sliding mode controller mainly includes two steps [45]: Firstly, an appropriate sliding mode surface is designed to make the state trajectory of the system have good dynamic characteristics such as asymptotic stability after entering the sliding mode. Then, the sliding mode control law is designed to make the state trajectory of the system move to the sliding mode surface and maintain the current motion.

The system of the controlled object can be converted into the form of equations of the nonlinear system, as follows:

$$\begin{cases} \dot{x}_1(t) = x_2(t) \\ \dot{x}_2(t) = f(x_1, x_2) + bu(t) + f \end{cases} \tag{15}$$

where x_1 and x_2 are state variables of the system; $f(x_1,x_2)$ is the nonlinear function of the system; $u(t)$ is the control input variable of the system; and f is the outside interference.

The sliding mode surface function designed in this paper is as follows:

$$s = ce + \dot{e}, \quad c > 0 \tag{16}$$

The error and its derivatives are defined as follows:

$$\begin{cases} e(t) = x_{1d} - x_1 \\ \dot{e}(t) = \dot{x}_{1d} - \dot{x}_1 = \dot{x}_{1d} - x_2 \end{cases} \tag{17}$$

where x_{1d} is the target value; x_1 is the actual value; and e is the difference between the target value and the actual value.

Taking the derivative of the sliding mode surface function and combining Formula (17), the following equation is obtained:

$$\begin{aligned} \dot{s} &= c(\dot{x}_{1d} - x_2) + (\ddot{x}_{1d} - \dot{x}_2) \\ &= c(\dot{x}_{1d} - x_2) + (\ddot{x}_{1d} - f(x_1, x_2) - bu(t) - f_z) \end{aligned} \tag{18}$$

In order to improve the dynamic response of the control system and reduce the chattering caused by sliding mode motion, the exponential reaching law is used in this paper to design the controller [46]. The specific expression of the exponential reaching law is as follows:

$$\dot{s} = -\varepsilon \cdot \mathrm{sgn}(s) - ps, \quad \varepsilon > 0, p > 0 \tag{19}$$

A sliding mode controller based on the exponential reaching law is designed by combining Equations (18) and (19). The specific expression is as follows:

$$u(t) = \left[c(\dot{x}_{1d} - x_2) + (\ddot{x}_{1d} - f(x_1, x_2) - f_z) + \varepsilon \cdot \mathrm{sgn}(s) + ps\right]/b \tag{20}$$

It is necessary to verify the stability of the controller. In order to make the system satisfy the arrival condition of the sliding mode and have certain stability, it is necessary to satisfy the Lyapunov stability condition. According to the Lyapunov stability principle [47], the stability of the sliding mode controller is verified. In order to prove the stability of the controller to the control system, the Lyapunov function is chosen as the following equation:

$$V = \frac{1}{2}s^2 \tag{21}$$

The derivative of Equation (21) is combined with Equation (20) to obtain the following equation:

$$\begin{aligned} \dot{V} = s\dot{s} &= s\left[c(\dot{x}_{1d} - x_2) + (\ddot{x}_{1d} - f(x_1, x_2) - bu(t) - f_z)\right] \\ &= s(-\varepsilon \cdot \mathrm{sgn}(s) - ps) = -\varepsilon|s| - ps^2 \end{aligned} \tag{22}$$

Since $\varepsilon > 0, p > 0$; therefore,

$$\dot{V} = s\dot{s} = -\varepsilon|s| - ps^2 \leq 0 \tag{23}$$

According to $\dot{V} \leq 0$, it can be seen that the system is made to satisfy the Liapunov stability condition by the design of the controller, and it is finally proved that the sliding mode controller is asymptotically stable [48]. In summary, through the stability analysis, it is proved that under the action of the controller, the error finally converges to 0, and the control system can reach the control target.

In the formula of the exponential reaching law, sgn(s) is a discontinuous function with ultra-high frequency switching characteristics. The image of the sign function sgn(s) is shown in Figure 15a. In the working process, due to the properties of the sign function, the output value of the controller will continue to jump, resulting in the chattering phenomenon. The persistent chattering problem will cause damage to the thruster. Therefore, the sliding mode controller is improved by using a saturation function instead of a sign function. The basic principle of the saturation function is to replace the discontinuous sign function with a continuous saturation function. A boundary layer is designed in the saturation function. Continuous control is used inside the boundary layer, and normal sliding mode control is used outside the boundary layer. The saturation function image is shown in Figure 15b. According to the image of the two functions, it can be seen that compared with the sign function, sat(s) is a continuous function, and the output value does not switch quickly. Replacing the sign function with saturation function can make the controller become a continuous controller, reduce the discontinuity of the controller output value, effectively weaken the chattering phenomenon, and improve the stability of the system.

The specific expressions of the sign function and the saturation function are as follows:

$$sat(s) = \begin{cases} 1 & s > 0 \\ 0 & s = 0 \\ -1 & s < 0 \end{cases}, \qquad sat(s) = \begin{cases} 1 & s > \Delta \\ ks & |s| \leq \Delta, k = 1/\quad \Delta \\ -1 & s < -\Delta \end{cases} \tag{24}$$

Therefore, the sliding mode controller based on the saturation function is as follows:

$$u(t) = \left[c(\dot{x}_{1d} - x_2) + (\ddot{x}_{1d} - f(x_1, x_2) - f_z) + \varepsilon \cdot sat(s) + ps\right]/b \tag{25}$$

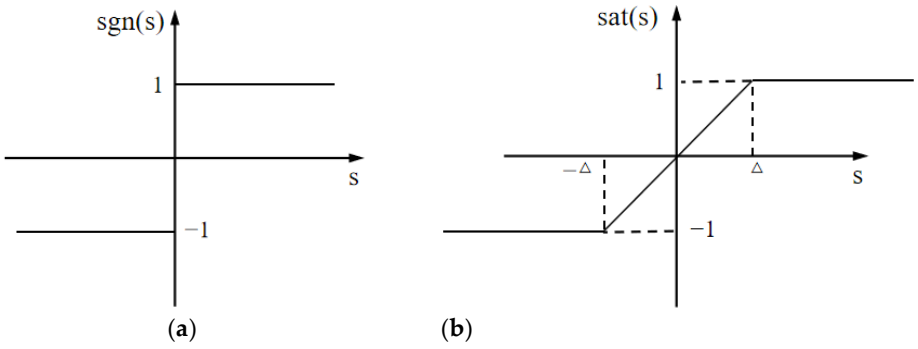

Figure 15. Graphs of functions. (**a**) Sign function; (**b**) saturation function.

7.2. Establishment of Simulation Model

When the amphibious robot swims underwater, keeping the depth constant or the heading angle constant is the premise of the stable operation of the amphibious robot. Therefore, it is very important to establish a fixed depth controller and a fixed heading controller.

In order to facilitate the design of the controller, the dynamic model of the two degrees of freedom of snorkeling and turning is transformed to obtain the following equations:

$$\begin{cases} \dot{z} = w \\ \dot{w} = f(w)w + b_Z\tau_Z + f_Z \end{cases} \tag{26}$$

$$b_Z = \frac{1}{m - Z_{\dot{w}}},\ f(w) = -\frac{Z_w + Z_{w|w|}\left|w\right|}{m - Z_{\dot{w}}}$$

$$\begin{cases} \dot{\psi} = r \\ \dot{r} = f(r)r + b_N\tau_N + f_N \end{cases} \tag{27}$$

$$b_N = \frac{1}{I_z - N_{\dot{r}}},\ f(r) = -\frac{N_r + N_{r|r|}\left|r\right|}{I_z - N_{\dot{r}}}$$

Therefore, according to Formulas (15) and (20), a fixed depth controller and a fixed heading controller are obtained, as follows:

$$\tau_Z = \left[c(\dot{x}_{1d} - x_2) + (\ddot{x}_{1d} - f(w)w - f_Z) + ps + \varepsilon \cdot \mathrm{sgn}(s)\right]/b_Z \tag{28}$$

$$\tau_N = \left[c(\dot{x}_{1d} - x_2) + (\ddot{x}_{1d} - f(r)r - f_N) + ps + \varepsilon \cdot \mathrm{sgn}(s)\right]/b_N \tag{29}$$

7.3. Simulation Results and Analysis of Fixed Depth Controller

In this section, the sliding mode controller and PID controller are simulated and compared for the fixed depth motion. First, the simulation system of two controllers is built, and then, the relevant expressions are written for different modules, and parameters are set. The model block diagrams of the simulation system are shown in Figures 16 and 17.

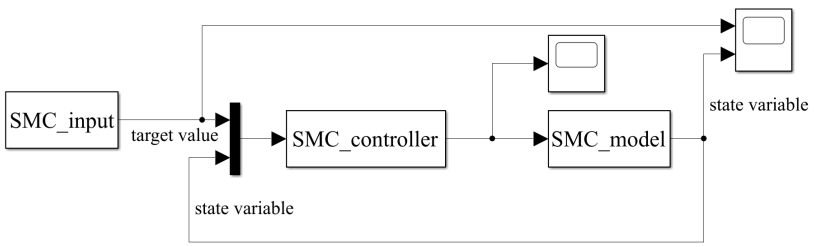

Figure 16. Simulation model block diagram of sliding mode control system.

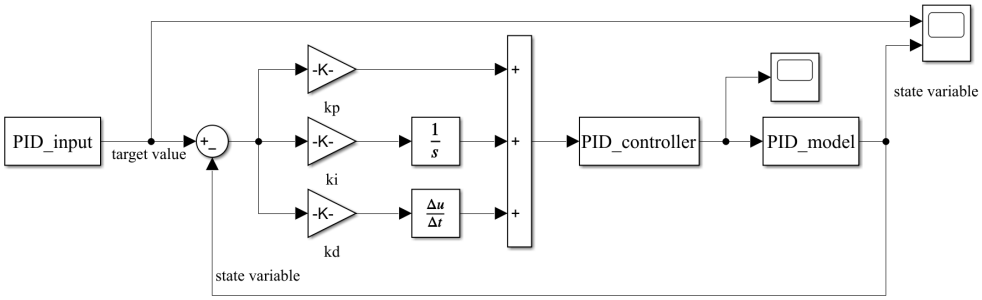

Figure 17. Simulation model block diagram of PID control system.

The initial depth of the amphibious robot is set to 0 m, and the target depth is set to 1 m. The simulation time is set to 40 s, and the simulation step size is set to 0.01 s. Based on the above parameters, the two control systems are simulated, and the simulation results are shown in Figure 18.

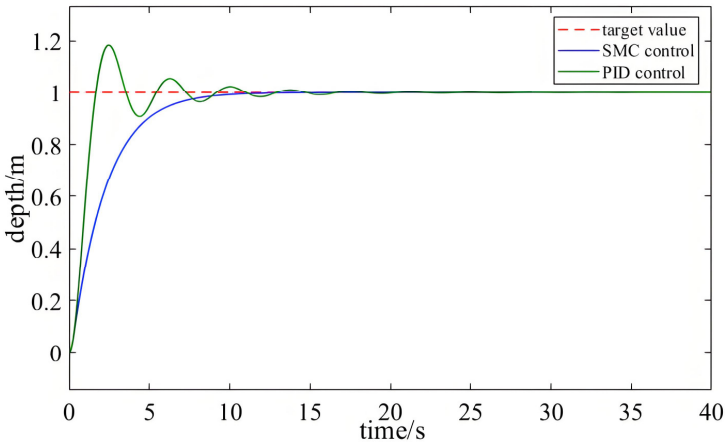

Figure 18. The simulation result of the fixed depth controller.

As shown in Figure 18, from a time point of view, the time required for the depth controlled by the sliding mode controller and the PID controller to reach a steady state is about 14 and 21 s. The sliding mode controller responds faster. From an overshoot point of view, the depth overshoot controlled by the PID controller is 21%, while the depth controlled by the sliding mode controller has no obvious overshoot. Before reaching the steady state, the depth value controlled by the PID controller has a gradual attenuation fluctuation. Therefore, the control process of the sliding mode controller is more stable. In summary, both controllers have excellent control performance in the simulation process of fixed depth motion. However, the sliding mode controller has better robustness and is more helpful in improving the working efficiency of the amphibious robot.

7.4. Simulation Results and Analysis of Fixed Heading Controller

The simulation model framework of the fixed heading controller is the same as that of the fixed depth controller. The expressions and parameters of different modules are changed. The initial heading angle of the amphibious robot is set to 0°, and the target heading angle is set to 45°. Other parameters such as the simulation time and simulation step size are kept unchanged. Based on the above parameters, the two control systems are simulated and analyzed, and the simulation results are shown in Figure 19.

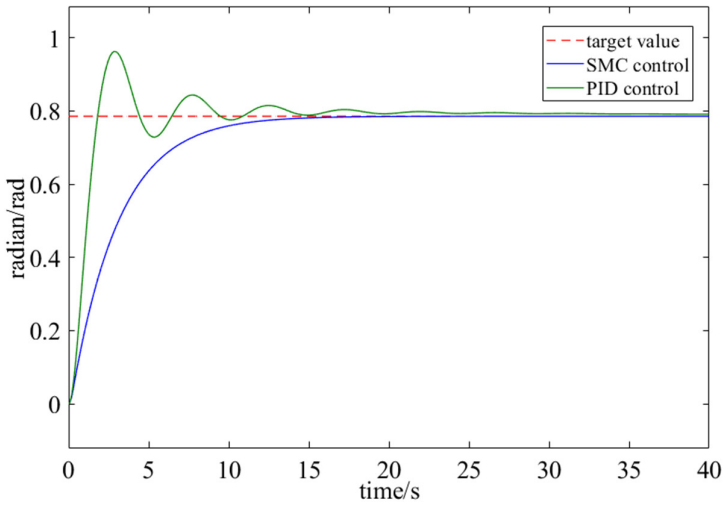

Figure 19. The simulation result of the fixed heading controller.

As shown in Figure 19, it takes about 20 s for the sliding mode controller to make the heading angle reach the target value. However, it takes about 25 s for the PID controller to get the heading angle to the target value. There is a steady-state error after the heading angle is stable, which is about 1°. The overshoot of the heading angle controlled by the PID control system is about 20%, and the heading angle oscillates from the maximum deviation angle to the stable state many times during the control process. Therefore, considering the control accuracy, response time, and stability, the sliding mode controller has better control performance than the PID controller for the fixed heading motion form of the amphibious robot.

8. Experiments

In order to verify the rationality of the structural system and the effectiveness of the control system, many experiments are designed and carried out. The experimental environment is land and underwater. The experimental platform includes an outdoor pool, a steel plate, and a steel pipe. Before the experiment starts, the basic functions of the various devices in the control system and the structural system are tested. The amphibious robot system and experimental environment are shown in Figure 20.

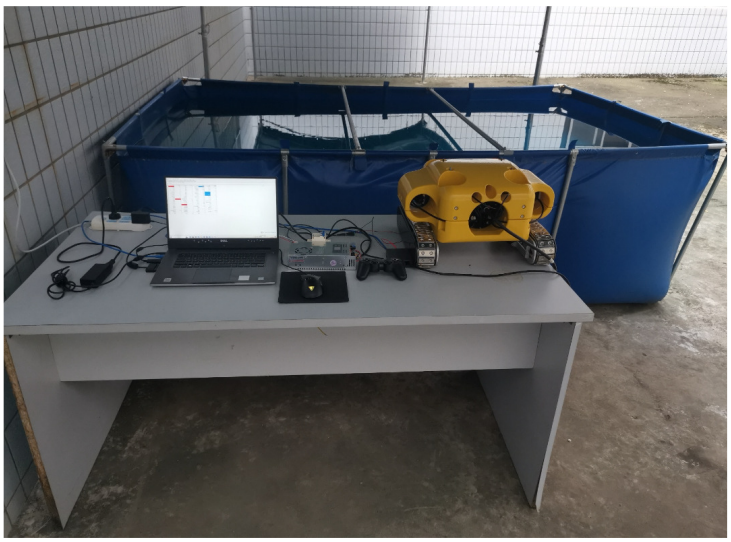

Figure 20. The amphibious robot system and experimental environment.

8.1. Crawling Motion Experiment

According to the previous theoretical analysis, when the metal structure is located in the air and the inclination angle is 0 degrees, the probability of instability of the amphibious robot is the highest. Therefore, the steel plate is placed in the air and fixed perpendicular to the ground, and then, the crawling performance of the amphibious robot is tested.

The crawling experiment process is shown in Figure 21. Firstly, the amphibious robot can be statically adsorbed onto the steel plate without slipping and overturning. Then, the remote control handle is operated to drive two waterproof motors to work. The amphibious robot can complete the basic motion forms such as forward, backward, and turning on the steel plate at a uniform speed. The crawling process is stable without slipping and overturning. The experimental results show that the structural design of the crawler chassis system is reasonable, and the performance of the two waterproof motors meets the motion requirements. In summary, the amphibious robot can meet the requirements of crawling motion on the metal wall in different environments and at different inclination angles.

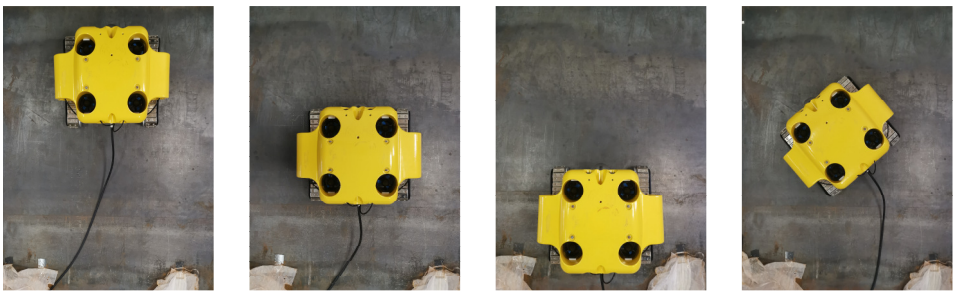

(**a**) (**b**) (**c**) (**d**)

Figure 21. Crawling experiment. (**a**) Forward state; (**b**) stationary state; (**c**) backward state; (**d**) turning state.

8.2. Floating Motion Experiment

In order to test the basic floating motion mode of the amphibious robot and the autonomous motion mode of fixed depth and fixed heading, the amphibious robot is placed in an outdoor pool for experiments.

Firstly, the buoyancy performance of the amphibious robot is tested and verified. The amphibious robot without the installation of working equipment is put into the pool and kept there for a few minutes to keep the amphibious robot in a static state. As shown in Figure 22, observing the state of the amphibious robot, it can be seen that the pitch angle of the amphibious robot is about 3°, and the roll angle is about 1°. The amphibious robot can reach a balanced state in the horizontal direction, which verifies that the design of the buoyancy module and the installation position of other equipment are reasonable. In order to test the buoyancy of the amphibious robot installed with work equipment, a 2 KG weight was used instead of work equipment and placed directly above the amphibious robot. As shown in Figure 22c, observing the state of the amphibious robot, it can be seen that the amphibious robot can be completely below the water surface and suspended in the water, showing a state of basically zero buoyancy. Finally, the weight was fixed to the bottom of the amphibious robot for subsequent experiments. In the future, when operational equipment is required, the weight will be removed, and operational equipment will be installed. In summary, the experimental test results of buoyancy performance are basically the same as the calculation results of the three-dimensional software (solidworks2023), and the amphibious robot can move and work stably underwater.

(**a**) (**b**) (**c**)

Figure 22. The test experiment of buoyancy performance. (**a**) The roll angle in the static state; (**b**) the pitch angle in the static state; (**c**) the state of zero or minimal buoyancy.

The process of floating motion is shown in Figure 23. The amphibious robot has weak buoyancy and can be suspended in water. The control instructions are sent to the underwater control system by the remote control handle. The control instructions are parsed by the control system to realize the basic floating motion forms of the amphibious robot, such as diving, moving forward, and turning.

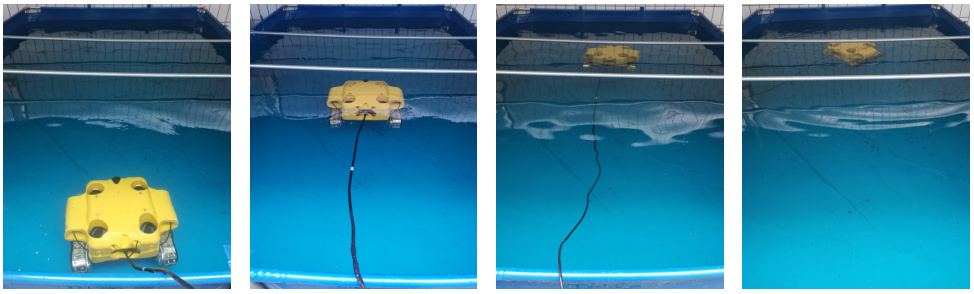

(**a**) (**b**) (**c**) (**d**)

Figure 23. Floating motion experiment. (**a**) Backward state; (**b**) diving state; (**c**) forward state; (**d**) turning state.

In the floating motion experiment, the amphibious robot can complete the basic floating motion forms underwater. The amphibious robot has a fast response speed, a stable motion process, and good flexibility, which can meet the basic floating motion requirements underwater.

In order to test the actual control effect of the sliding mode control algorithm, two experiments of fixed depth motion and fixed heading motion are carried out in the outdoor pool. The target depth and target angle are set to the same value as the simulation system. The target value is sent to the underwater control system through the overwater control software. Each experiment is carried out many times, and then the average value of multiple sets of experimental data collected by the sensor is drawn into a curve. The curves of the simulation results and experimental results are drawn in an image for comparison, as shown in Figure 24.

The results of the fixed depth motion experiment are shown in Figure 24a. The amphibious robot can reach the target depth quickly, and the use time is about 17 s. There is a slight fluctuation in the depth value before the amphibious robot is relatively stable, and the fluctuation range is about 6 cm.

The experimental results of fixed heading motion are shown in Figure 24b. The amphibious robot takes about 22 s to turn to the target heading angle. Before reaching the target heading angle, the fluctuation range of the actual heading angle is about 5°.

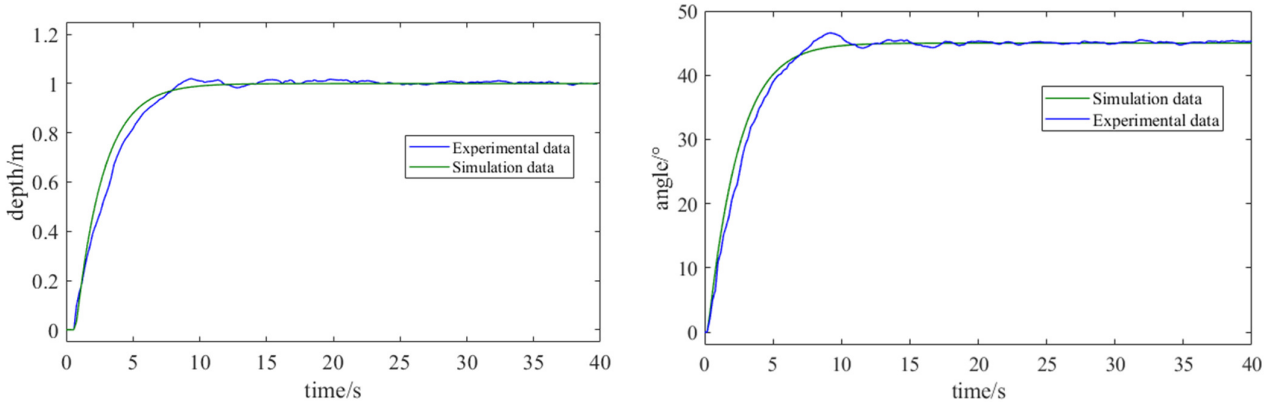

(**a**) (**b**)

Figure 24. Comparison of simulation data and experimental data. (**a**) Depth change curve; (**b**) heading angle change curve.

In summary, the steady-state error and overshoot of the two experimental results are relatively small, and the motion process is relatively stable, which will not have much impact on the work of the amphibious robot. From the comparison of the curves in Figure 24, it can be seen that the curve variation trend of experimental results and simulation results is the same. The time used in the experiment was slightly longer than the time used in the simulation before reaching the set goal. Therefore, the experimental control effect of the sliding mode control algorithm shows good robustness and stability, which can meet the underwater working requirements of the amphibious robot.

Due to the simplification of the system model, the error of model parameters, and the irregularity of external interference, there is error between the simulation results and the experimental results, and the curve of the experimental results is not as smooth as that of the simulation results. Due to the error of the sensor and the delay of data transmission, the experimental results have a small range of fluctuations. Therefore, in order to reduce the error between the experimental results and simulation results in the future, the following methods will be adopted for optimization: optimizing the assumptions and processing of the model, improving the accuracy of model parameters and controller parameters, improving the standard degree of experimental operation, selecting sensors and other devices with better performance, increasing the number of experiments, adding noise reduction processing and compensation control, etc.

8.3. Simulation Experiment of Application Scene

The amphibious robot can be applied to the safety inspection and maintenance of marine engineering facilities. Therefore, the simulation experiment of the application scene in this section is carried out. The shape of most marine engineering facilities is a cuboid or a large-diameter cylinder, and the material is high-strength steel, as shown in Figure 1. Therefore, a steel plate is used as the target object of the amphibious robot climbing a wall. At the same time, a steel pipe with a diameter of 12 cm is used as the target object of the amphibious robot swimming underwater. First, marks are made on the surface of the steel plate and the steel pipe to indicate the location of the damage to the structure. The steel plate and the steel pipe are then placed in the outdoor pool.

According to the camera screen, the remote control handle is operated to make the amphibious robot swim near the steel pipe, and a full range of safety inspections of the steel pipe is carried out, as shown in Figure 25a. After the damage position of the steel pipe is found, the depth and attitude of the amphibious robot are controlled by the fixed depth and fixed heading function to ensure that the camera screen is stably aligned to the defect position, as shown in Figure 25b. The damaged location is photographed and saved, and

the depth data and attitude data are recorded at this time to provide location information for subsequent maintenance.

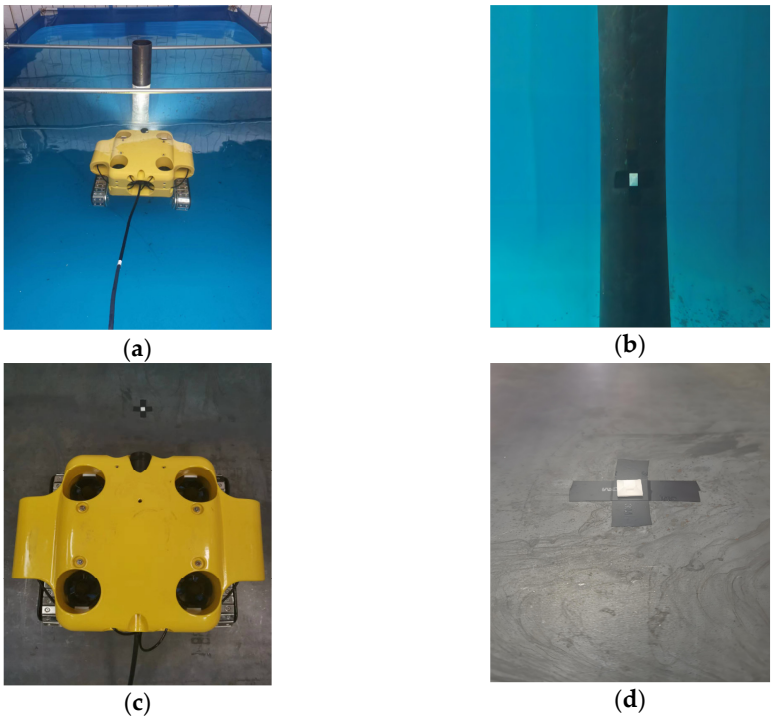

Figure 25. Application scene simulation experiment. (**a**) swimming process; (**b**) steel pipe defect location; (**c**) climbing process; (**d**) steel plate defect location.

When the metal structure above the waterline needs to be checked for safety, the thruster is controlled by the remote control handle to make the amphibious robot adsorb onto the steel plate below the waterline. The pitch angle of the single-degree-of-freedom pan–tilt camera is adjusted to make the camera face the steel plate at the front end of the amphibious robot. Then, driven by two waterproof motors, the amphibious robot crawls onto the steel plate above the waterline. The safety inspection of the steel plate is carried out in different crawling directions, as shown in Figure 25c. After finding the defect position of the steel plate, the amphibious robot stops crawling; the defect position is photographed, as shown in Figure 25d.

At the same time, the buoyancy module of the amphibious robot reserves an installation hole. If it is necessary to carry out the water jet cleaning and probe inspection of offshore engineering facilities, the corresponding equipment can be installed at the installation hole, and the work can be carried out according to the above operation process.

9. Conclusions

In this paper, a small modular amphibious robot system, including a structural system and a control system, is developed for application requirements such as the safety inspection and maintenance of marine engineering facilities. The objectives of the modular design of the structure, composite motion modes of floating and crawling, stable adsorption of the crawling mode, and self-adaptation to crawling walls were achieved by means of mechanical analysis, modeling software, and finite element software. The detailed design of the control system, including hardware and software, was completed by means of electronic design technology and programming software. The simulation and experimental results show that all parts of the amphibious robot meet the strength requirements of 100 m underwater. The buoyancy module of the amphibious robot generates 20 N more than the gravity of the amphibious robot, in order to balance the gravity of the operational equipment to be installed in the future. The crawling speed of the amphibious robot can

reach 3.5 m/min, and the swimming speed can reach 1 m/s. In the crawling mode, the amphibious robot can be reliably adsorbed onto a steel plate perpendicular to the ground without slipping and overturning. The crawling process of the amphibious robot is stable, and the actions of forward motion, backward motion, and turning are realized. In the floating mode, the amphibious robot can complete diving, advancing, turning, pitching, and other actions. The swimming process is stable, and the action is flexible. The motion performance of the two working modes can meet the basic needs of the work.

In order to realize the autonomous motion function of fixed depth and fixed heading, a sliding mode control algorithm combining exponential reaching law and saturation function is designed. The simulation results show that in the simulation of the autonomous motion of fixed depth and fixed heading, the time used by the sliding mode controller is about 6 s and 5 s less than that used by the PID controller, respectively. In the simulation of two kinds of autonomous motion, the amount of overshoot generated by the target controlled by the PID controller reaches 21% and 20%. The control target of the sliding mode controller has almost no overshoot. The sliding mode control algorithm has a faster response speed and better stability than the PID control algorithm. The experimental results show that in the experiments of the autonomous motion of fixed depth and fixed heading, the time used by the sliding mode controller is 16 s and 22 s, and the fluctuation range is about 6 cm and 5°, respectively. The sliding mode control algorithm control process is relatively smooth, and the fluctuation is relatively small. The curve change trend of the experimental results is the same as that of the simulation results. In the two kinds of autonomous motion, the time used in the experiment is about 2 s longer than that used in the simulation. Therefore, the sliding mode control algorithm can improve the attitude stability and work efficiency of the amphibious robot.

Finally, a simulation experiment of the application scenario is carried out. In the floating mode, the amphibious robot can smoothly and flexibly perform a safety inspection on a steel pipe and accurately photograph and record the defect location. Similarly, in the crawling mode, the amphibious robot is able to crawl steadily through the underwater and overwater portions of a steel plate and find the defect locations. The amphibious robot has an installation hole which can be equipped with manipulators, cleaning guns, probes, and other equipment to complete different operational tasks in the future.

After two stages of development and experiments, some shortcomings, limitations, and future challenges of the amphibious robot system are summarized. For example, the overall weight and volume of the system is relatively large, and greater adsorption force is required during crawling. The crawler chassis system is not designed with a cushioning structure, which can cause slight damage to the overall structure of the amphibious robot. The parameter estimation of the system model is not completely accurate, and there are errors with the actual situation. The resolution of the underwater camera is low, and the details of the underwater target cannot be clearly obtained. The signal interference and the underwater noise are large, and the accuracy of various sensors is relatively poor. The degree of autonomy and intelligence is relatively low, and a lot of manual operation is required. In the future, the above shortcomings, limitations, and challenges will be improved and optimized. The overall appearance of the system will be optimized to further reduce the air resistance and water flow resistance. Materials with lower density and greater strength will be selected to reduce the overall weight of the system. More accurate model parameters and controller parameters will be obtained through multiple simulations and experiments to reduce the error with the actual model. An underwater camera with a higher definition will be selected, and image processing technology and target recognition technology will be developed to improve the intelligence and autonomy of the system. A control motherboard with a higher performance and a sensor with higher precision will be selected, and filter noise reduction technology will be developed to reduce the underwater signal interference and improve the stability of the control system.

Author Contributions: Data curation, Z.W.; investigation, F.R.; methodology, Z.W.; project administration, F.R.; resources, F.R.; software, Z.W.; supervision, Z.W.; validation, F.R.; writing—original draft, Z.W.; writing—review and editing, F.R. All authors have read and agreed to the published version of the manuscript.

Funding: Hainan Province Science and Technology Special Fund, the specific research fund of The Innovation Platform for Academicians of Hainan Province (YSPTZX202301); High-tech project of Hainan Province, Intelligent ROV R&D and application technology of integrated inspection operation (ZDYF2023GXJS004); Scientific Research and Technology Development Project of China National Petroleum Corporation Limited, Research on Development of Intelligent ROV System and Supporting Technology of Jacket Operation (2021DJ2504).

Data Availability Statement: The data are unavailable due to privacy or ethical restrictions.

Conflicts of Interest: The authors declare no conflict of interest. The funding sponsors had no role in the design of this study; in the collection, analyses, or interpretation of data; in the writing of this manuscript, and in the decision to publish the results.

References

1. Zhong, C.; Du, P.; Liu, Z.L.; Zhu, S.B.; Qian, P.Y. Interconnection between carbon neutrality and development of offshore oil and gas in China. *Chem. Eng. Oil Gas* **2023**, *52*, 32–40+47.
2. Zhu, J.S.; Yang, Q.Q.; Liu, W.; Feng, S.H. Technology development research and standardization suggestions for submersibles. *Shipbuild. Stand. Qual.* **2023**, *4*, 15–18.
3. Ye, C.; Cao, J.; Liu, S. Innovation and development of foreign manned deep submergence technology. *Ship Sci. Technol.* **2023**, *45*, 1–7.
4. Wu, Y.S.; Si, M.C.; Zhu, Z.; Li, L.; Ni, T. Key development directions of marine science and technology. *Sci. Technol. Foresight* **2022**, *1*, 20–35.
5. Ren, C.; Li, N.; Du, Z.P. Research Status and Development Trend of Deep-sea AUV/ARV. *Digit. Ocean. Underw. Warf.* **2023**, *6*, 63–71.
6. Huang, X.T.; Jia, F.X.; Xiao, Z.H.; Zhang, T.D.; Lei, M.; Luo, W.Z. The application status and key technologies of autonomous underwater vehicles in polar regions. *Ship Sci. Technol.* **2024**, *46*, 1–9.
7. Zhang, Y.J. Analysis of large AUVs and surface reconnaissance technology. *Digit. Ocean Underw. Warf.* **2023**, *6*, 406–412.
8. Chao, X.L. Application of portable AUV in underwater special operations. *Ship Electron. Eng.* **2023**, *43*, 29–32.
9. Li, K.X. ROV: Science and technology envoys of exploring the deep blue. *Robot Ind.* **2024**, 40–44. [CrossRef]
10. Liu, Z.X. Hanhai Lanfan: Ploughing the deep sea, sailing for a new era. *Robot Ind.* **2024**, 53–57. [CrossRef]
11. Wu, C.B. Shandong Future: Underwater robots accelerate deep sea exploration. *Robot Ind.* **2024**, 62–64. [CrossRef]
12. Zhang, H.H.; Zhang, B.L.; Sun, B. Structural design and optimization of small ROV for shallow water observation. *Ship Ocean Eng.* **2023**, *52*, 62–65.
13. Zhang, J.Q.; Xie, Y.H.; Li, D.T.; Gao, W.P.; Chen, Q.; Wang, J.; Wang, Y.J.; Hong, Y.Q. Structural design and research of underwater robot for aquaculture ship operation. *South China Fish. Sci.* **2024**, *20*, 11–24.
14. Yuan, Q.; Zhou, D.; Hu, B.; Wang, H.L.; Zhu, L.; Tong, L.; Sun, T.; Wang, L.Y. Design and implementation of the observation-level underwater robot inspection device in clean water tank. *China Water Wastewater* **2024**, *40*, 105–109.
15. Cui, X.F.; Lin, H.T.; Qu, X.W.; An, N.N. Structural design and simulation of underwater vehicle for ship inspection. *Ship Eng.* **2024**, *46*, 153–156.
16. Cao, Y.W.; Chou, Y.X.; Shen, M.Y. Design of an underwater robot for the inspection of oil pipelines in forestry. *For. Mach. Woodwork. Equip.* **2024**, *52*, 88–91.
17. Wang, J.R.; Zhang, J.Y.; Li, C.; Qin, M.H. Research and experiment of small-sized autonomous underwater robot for pipeline inspection in shallow water. *J. Mach. Des.* **2023**, *40*, 83–87.
18. Wang, X.; Luo, T.; Lei, Y. Design and analysis of crawling robot for underwater structure detection. *Technol. Highw. Transp.* **2023**, *39*, 74–82.
19. Zhao, F. Design and adsorption analysis of tracked underwater observation robot. *Mach. Tool Hydraul.* **2024**, *52*, 134–141.
20. Huang, H.X.; Wang, Z.; Cheng, S.S.; Li, C.M. Optimized design of the main structure of a wall-climbing robot for bridge detection based on negative pressure adsorption. *J. South China Univ. Technol.* **2023**, *51*, 21–33.
21. Han, L.C.; Wang, L.M.; Xue, Y.Q.; Hou, J.X. Modeling and simulation analysis of new rigid-flexible coupling wall-climbing robot's virtual prototype. *J. Mach. Des.* **2024**, *41*, 42–51.
22. Wang, D.; Li, H.L. Structural Design Analysis and Simulation of Flexible Terminal Quadruped Wall-Climbing Robot. *Control. Eng. China* **2024**, 1–7. [CrossRef]
23. Wang, X.M.; Li, T. Analysis on cleaning performance and experiment of underwater cleaning robot for surface. *J. Jilin Univ.* **2023**, *53*, 3062–3068.
24. Zhu, W.L.; Liu, M.J.; Wang, Z.P.; Guo, S.K. PID control system design of underwater robot. *Marit. Saf.* **2024**, *6*, 1–3.

25. Wang, Z.Y.; Li, W.B.; Xu, D.C.; Bai, X.P.; Guo, P. Design and motion control experimental of lawn maintenance robot. *For. Eng.* **2024**, *40*, 178–183+196.
26. Guo, Z.K.; Wang, Y.H.; Yao, Z.G.; Li, R.Z. Design and implementation of automatic line patrol robot based on PID control algorithm. *Autom. Appl.* **2024**, *65*, 54–56.
27. Li, L.J.; Zhang, H.; Li, X.Q.; Li, Q.Y.; Yao, J.F. The algorithm design of robot tracking control based on improved neural network. *Mach. Des. Manuf. Eng.* **2024**, *53*, 75–78.
28. Liu, E.C.; Liu, T.Y. Robot fuzzy control algorithm based on wavelet neural network. *Ind. Instrum. Autom.* **2023**, *4*, 84–88.
29. Zhang, D. Course controller design of unmanned ship based on neural network. *Ship Electron. Eng.* **2024**, *44*, 67–69.
30. Li, C.Y.; Wang, W.; Geng, B.K.; Hu, K.R.; Wang, Y.C. Neural robust adaptive sliding mode method for spacecraft attitude control with input saturation. *J. Astronaut.* **2024**, *45*, 1269–1280.
31. Wang, H.X.; Chen, M.S.; Cao, W.J. Research on stability of gait control for bionic quadruped robots. *Wirel. Internet Sci. Technol.* **2024**, *21*, 60–62.
32. Brantner, G.; Khatib, O. Controlling Ocean One: Human–robot collaboration for deep-sea manipulation. *J. Field Robot.* **2021**, *38*, 28–51. [CrossRef]
33. Wu, J.G.; Ren, Z.G.; Lv, R.H. Development and application of modular autonomous underwater vehicle. *J. Mar. Inf. Technol. Appl.* **2022**, *37*, 10–20.
34. Xu, D.Y.; Ling, H.J. A closed streamlined observation stage ROV design. *Ship Sci. Technol.* **2018**, *40*, 143–148.
35. Sun, Z.N.; Wang, Y.L.; Lin, S.C.; Jin, Z.G. Analysis of magnetic force influencing factors of permanent magnet adsorption wall-climbing robot. *Mach. Des. Manuf.* **2024**, *4*, 368–372.
36. Zhao, J.Y.; Zhang, Y.N.; Bi, X.D.; Yan, C.X.; Dong, Y.F. Optimum design of magnetic adsorption structure and machine performance test for sand blasting and rust-removing wall-climbing robot. *J. China Univ. Pet. (Ed. Nat. Sci.)* **2020**, *44*, 94–99.
37. Guo, G.G. The Research on Adaptive Permanent Magnetic Adsorption Wall Climbing Robot Technology. Master's Thesis, Northeast Petroleum University, Daqing, China, 2020.
38. Chen, J.K. Design and Research of Wall-Climbing Robot for Cargo Hold Cleaning. Master's Thesis, University of Chinese Academy of Sciences, Beijing, China, 2022.
39. Luo, Y.H.; Wu, J.M.; Zhou, H.F. Trajectory tracking control of underwater vehicle based on hydrodynamic parameters calculated by CFD. *Chin. J. Ship Res.* **2022**, *17*, 237–245+272.
40. Wei, Y.H.; Zhou, W.X.; Jia, X.Q.; Wang, Z.P. Model decoupling and multi-controller joint control of horizontal movement for AUV. *J. Huazhong Univ. Sci. Technol. (Nat. Sci. Ed.)* **2016**, *44*, 37–42.
41. Liu, J.; Yan, J.L.; Liu, Q.; Ye, H.C.; Wang, Z.Y.; Hu, Q. Research on ROV attitude control technology based on thrust vector allocation. *J. Jilin Univ. (Inf. Sci. Ed.)* **2024**, *42*, 249–259.
42. Han, L.; Shi, X.X. Research on Design and Motion Control of Six Degrees of Freedom Underwater Robot. *J. Nanjing Inst. Technol. (Nat. Sci. Ed.)* **2021**, *19*, 7–12.
43. Liu, C. The Depth Control and Surface Monitoring System Design on an Abdominal Operating ROV. Master's Thesis, Huazhong University of Science & Technology, Wuhan, China, 2017.
44. Liu, S.Y. Research on the Sliding Mode Control of Semi-Submersible Vehicle at High Sea Conditions. Master's Thesis, China Ship Research and Development Academy, Beijing, China, 2017.
45. Hu, L. Research and Implementation of AUV Station Keeping Control for Submarine Cable Inspection. Master's Thesis, Hangzhou Dianzi University, Hangzhou, China, 2023.
46. Tang, Q.R.; Deng, Z.Q.; Li, Y.H.; Chen, D. Trajectory tracking of an underwater vehicle-manipulator system based on sliding mode control with exponential reaching law. *Ship Sci. Technol.* **2019**, *41*, 54–58.
47. Wang, X.Y. Port Operation ROV System Integration with Lifting Module and Motion Control Research. Master's Thesis, Harbin Engineering University, Harbin, China, 2022.
48. Liu, J.L. Control System Research on Spherical Underwater Robot with Flywheel Steering Apparatus. Master's Thesis, Beijing University of Posts and Telecommunications, Beijing, China, 2016.